RESEARCH ARTICLE

Ovary-derived Decellularized Extracellular Matrix-based Bioink for Fabricating 3D Primary Ovarian Cells-laden Structures for Mouse Ovarian Failure Correction

Jiahua Zheng[1], Yibin Liu[1], Chenxiao Hou[1], Zhongkang Li[1], Shaopeng Yang[2], Xiao Liang[3], Liang Zhou[4], Jiangbo Guo[5], Jingkun Zhang[1]*, Xianghua Huang[1]*

[1]Department of Obstetrics and Gynecology, The Second Hospital of Hebei Medical University, Shijiazhuang, Hebei, China
[2]Department of Gastroenterology, The Second Hospital of Hebei Medical University, Shijiazhuang, Hebei, China
[3]Department of Obstetrics and Gynecology, College of Integrated Traditional Chinese and Western Medicine, Hebei University of Chinese Medicine, Shijiazhuang, Hebei, China
[4]Department of Reproductive, The Second Hospital of Hebei Medical University, Shijiazhuang, Hebei, China
[5]College of Science, Hebei Research Center of Pharmaceutical and Chemical Engineering, Hebei University of Science and Technology, Shijiazhuang, Hebei, China

Abstract: Fertility preservation is becoming a clinical duty in practice. Three-dimensional (3D) bioprinting technology is potentially realize ovarian morphological repair and reproductive endocrine function rebuild. There is no published work on 3D bioprinting ovary using a decellularized extracellular matrix (dECM)-based bioink, though dECM is the preferred matrix choice for an artificial ovary. The study aimed to explore swine ovarian dECM-based bioink to fabricate 3D primary ovarian cells (POCs)-laden structures for mouse ovarian failure correction. In this study, the ovarian dECM was converted to dECM-based bioink by dECM solution mixed with a seaweed gelatin blend solution of bioink that was characterized using scanning electron microscopy, circular dichroism, rheology, hematoxylin and eosin staining, and immunohistochemistry. The 3D scaffolds were, then, printed with or without POCs by the extrusion 3D bioprinter. The laden POCs viability was detected with the live/dead assay kit. A female castrated mouse model was established, and the mice were treated with five different methods. The results revealed that the 3D scaffold encapsulating POCs group had more positive signals in neoangiogenesis, cell proliferation and survival than the 3D scaffold group, and ensured sex hormone secretion. Meanwhile, the expression of germ cells in the 3D scaffold encapsulating POCs group was more intensely than the non-printed hydrogel encapsulating POCs group. The work shows that the 3D bioprinting ovary employing ovarian dECM-based bioink is a promising approach for ovarian failure correction.

Keywords: 3D bioprinting; Ovary; Decellularized extracellular matrix; Bioink; Primary ovarian cells

***Correspondence to:** Xianghua Huang, 215 Heping West Road, Shijiazhuang, Hebei, 050000, China; huangxh2003@163.com; Jingkun Zhang, 215 Heping West Road, Shijiazhuang, Hebei, 050000, China; zhangjingk110110@163.com

Received: March 09, 2022; **Accepted:** May 29, 2022; **Published Online:** July 26, 2022

(This article belongs to the *Special Issue: 3D Printing in Tissue Engineering*)

Citation: Zheng J, Liu Y, Hou C, *et al*., 2022. Ovary-derived Decellularized Extracellular Matrix-based Bioink for Fabricating 3D Primary Ovarian Cells-laden Structures for Mouse Ovarian Failure Correction. *Int J Bioprint*, 8(3): 597. http://doi.org/10.18063/ijb.v8i3.597

1. Introduction

Fertility issues have become a crucial problem to an increasing number of women of reproductive age with malignancies[1]. While cryopreservation and transplantation of ovarian tissue is increasingly recognized as a method to restore fertility, it is not an infallible method for certain types of cancer cells due to the risk of implantation[2]. In recent years, tissue engineering techniques may provide an approach to solve the clinical problems by constructing

bioengineered ovaries with an appropriate cell- and tissue-specific bioinks.

Bioengineered ovaries must mimic natural organs. Besides isolated follicles, it also requires autologous ovarian cells, which are required for follicle survival[3]. The follicles are separated from the stromal elements by encapsulating themselves in a basement membrane, and autologous ovarian cells are derived from cured ovarian samples[4]. Thus, it can be considered a safer means of restoring fertility in women with cancer.

Today, the materials used to construct bioengineered ovaries include both natural and synthetic polymers[5,6]. However, studies reported that the matrix of choice for artificial ovaries is the decellularized extracellular matrix (dECM)[7], because synthetic polymeric materials do not possess every property of dECM[8]. Ovary dECM materials for bioengineering ovaries have produced some promising results. Laronda *et al*.[9] first successfully constructed scaffolds from acellular bovine and human ovarian tissues to support follicle growth and restoration of ovarian function in ovariectomized mice. Another study produced a decellularized porcine ovarian matrix that supported the survival of rat granulosa cells in vitro and improved estradiol hormone secretion[10]. Hassanpour *et al*.[11] seeded rat primary ovarian cells (POCs) on the decellularized human ovarian matrix and found follicle-like structures within the matrix 4 weeks after transplantation. Pors *et al*.[12] investigated human preantral follicles seeded on the human ovary dECM. In vivo assessment showed that the survival of follicle was higher in the decellularized human ovarian scaffolds after 3 weeks of xenografting in mice. Despite these promising results with ovarian dECMs, it is challenging to find a precise fit with follicles of different sizes in the pores of dECMs. An alternative approach is to convert ovarian dECMs into a temperature-sensitive hydrogel. This method can perfectly encapsulate isolated follicles or other ovarian cells while maintaining acellular ovarian tissue components. Chiti *et al*.[13] converted bovine ovarian dECMs into hydrogel and demonstrated that mouse preantral follicles were able to survive in the hydrogel.

The traditional tissue engineering techniques described above, such as seeding cells on dECMs or encapsulating cells in hydrogels, can mimic physiological ovarian tissue and improve ovarian function to some extent. However, precise control of the spatial distribution, oxygen diffusion, or cell structure between cells and matrix remains a challenge for conventional tissue engineering. A solution to these problems are three-dimensional (3D) bioprinting technology[14]. 3D bioprinting technology has the potential to achieve ovarian morphological repair and reproductive endocrine function rebuild. The material used for 3D bioprinting is called "bioink." Bioink consists of individual living cells or living cells with a supporting hydrogel component[15]. At present, there is no published work on 3D bioprinting of ovaries using bioink composed of dECMs. However, 3D bioprinting should not be confused with 3D printing of biomaterials. The former refers to the printing process of live cells, while the latter refers to the printing of biomaterials, which does not require live cell printing (the printed scaffolds can be seeded with live cells)[16]. The 3D-bioprinted cell-loaded scaffolds possess ideal spatial distribution. Thus, we hypothesize that 3D bioengineering ovarian constructs using ovarian dECM-based bioink for tissue infiltration and target tissue remodeling will facilitate cell distribution and survival.

In this study, we focused on 3D bioprinting porous cylindrical-shaped ovarian constructs employing swine ovarian dECM-based bioink encapsulating POCs to evaluate the efficacy of ovarian failure correction.

2. Materials and methods

2.1. Animals

One hundred and twenty slaughterhouse-raised female swines (95 – 100 kg, aged 6 months) were used to harvest the fresh ovary tissues. Twelve female Kunming mice (16 – 20 g, aged 8 weeks) were used to determine the biocompatibility of the dECM-based bioink. One hundred and ninety female Kunming mice (13 – 15 g, aged 4 weeks) were used to prepare the POCs and animal model. All procedures involving animals were conducted in compliance with the guidelines of the local animal ethics committee on animal care (No. 2019-P060).

2.2. Decellularization of ovarian tissues

Fresh swine ovarian tissues decellularization was conducted based on previous work[17]. First, the ovaries were cut into pieces (3 mm thick), cleaned with normal saline, and treated with phenylmethylsulfonyl fluoride (PMSF) solution (0.1 mM/L) in a shaker (130 rpm) for 48 h at 4°C, which could inhibit protease activity. Second, the tissues were placed into a hypotonic Tris buffer (pH 8.0) containing 0.1% sodium dodecyl sulfate (SDS) and 0.1 mM/L PMSF for 12 h at 4°C. Third, the tissues were submerged in Tris-buffered saline containing 0.1 mM/L PMSF and 1% Triton X-100 solution by continuous shaking (130 rpm) at 4°C for 7 days. Fourth, the tissues were soaked in nuclease solution (pH 7.5) containing 50 U/ml deoxyribonuclease I (Sigma, Poole, UK) and 1 U/ml ribonuclease A (Sigma, Poole, UK) by shaking (80 rpm) at 37°C for 12.5 h. Then, the tissues were immersed in 0.1% peroxyacetic acid and 20% ethanol at 4°C for 2 h, and finally freeze-dried. The ovarian dECM was then formed.

2.3. Decellularization evaluation

The residual DNA content of the dECMs was measured to evaluate the degree of decellularization. The total DNA was extracted using TIANamp genomic DNA kit (Tiangen, Beijing, China). The DNA concentration was quantified by NanoDrop 2000 spectrophotometry (Thermo Scientific, USA) and the size of the remaining DNA fragments was verified by gel electrophoresis.

Fresh ovarian tissues and the dECMs were embedded in paraffin. The cell residues in the tissues were detected using hematoxylin and eosin (H&E) staining and 4,6-diamidino-2-phenylindole (DAPI) staining. The dECMs components such as collagen and proteoglycan were assessed by Masson staining and toluidine blue (TB) staining. The presence of proteins or peptides was detected by SDS–polyacrylamide gel electrophoresis (SDS-PAGE). Routine electrophoresis, dyeing, and discoloration were performed in turn. The microstructure of the dECMs was observed using scanning electron microscopy (SEM; JSM-5600LV, JEOL).

2.4. Preparation of dECM-based bioink

The dECMs were pulverized using a small grinder with the help of liquid nitrogen. 100 mg dECM powder was taken, 3 ml hydrochloric acid solution (pH 2.0) and 60 mg pepsin were added to the dECM powder and digested at 37°C for 24 h. The dECM solution pH was adjusted using NaOH solution (10 M) (from 3.2 – 3.5 to 7.0 – 7.2) after solubilization. Then, 2 ml tri-distilled water was added into 15% (w/v) gelatin and 3% (w/v) sodium alginate (Sigma-Aldrich; Merck) and dissolved at 55°C for 30 min. Finally, dECM-based bioink working solution was produced by mixing 3 ml dECM solution (pH 7.0 – 7.2) with the above 2 ml solution.

2.5. The biochemical characterization and biocompatibility of the dECM-based bioink

(1) Microarchitecture of the dECM-based bioink by SEM

SEM was performed to observe the microarchitecture of the bioink. First, the bioink was freeze-dried and then fixed in 2.5% glutaraldehyde at 4°C for 12 h. Second, the above samples were sequentially immersed in 70%, 80%, 90%, and 100% ethanol for 15 min. The samples were then coated with gold sputter and viewed under SEM.

(2) Circular dichroism (CD) spectra properties

To evaluate the protein structures and thermal stability of the bioink, we tested the bioink with CD, including room temperature CD and the variable temperature CD analysis. First, the baseline was measured, followed by the room temperature CD. The scanning speed was 60 nm, scanning band was 190 – 260 nm. The average of three scan results after subtracting the baseline is the ellipticity. According to the results of CD at room temperature, the variable temperature CD analysis was performed. The detection wavelength was 199 nm, the starting temperature was 30°C, the ending temperature was 90°C, and the heating rate was 1°C/min. The thermal denaturation curve was, then, analyzed by a fitting equation model (a sigmoid curve) to obtain the thermal denaturation temperature (Tm) value.

(3) Rheological characterization

To assess the viscosity and the strain sweep of the bioink (before and after cross-linking of calcium chloride) and the dECM solution (pH 3.2 – 3.5), we conducted rheological investigation on a rotation rheometer (Malvern Kinexus Ultra+) at 25°C. Amplitude sweep (0.01 – 100 strain, 10% rad/s) was performed to assess the strain dependent storage modulus (G') and loss modulus (G'').

(4) Biocompatibility of the dECMs bioink in vivo

Twelve 8-week-old female Kunming mice were subcutaneously injected with 400 μl bioink on the back of each mouse. The injections were taken at the 1st, 2nd, 4th, and 9th week for H&E staining and immunohistochemistry (IHC) Staining (CD45, an inflammatory marker).

2.6. Isolation of the POCs

According to Hassanpour *et al*.'s protocol[11], POCs were prepared from 4-week-old female Kunming mice and then encapsulated in the bioink. Briefly, each mouse was intraperitoneally injected with 10 IU Pregnant Mare Serum Gonadotropin (PMSG, Solarbio) followed by 16 U Chorionic Gonadotrophin for Injection (Harbin Sanma Animal Pharmaceutical Co. LTD) after 48 h, and then, the ovaries were isolated after 6 h. The ovaries were incubated in α-MEM medium (Gibco) with 1% penicillin-streptomycin (PS, Millipore) at 4°C. Afterward, the ovaries were, manually, dissected with fine needles into smaller fragments and incubated in a digestion solution consisting of Dispase II (Cat. No. D4693-1G, Sigma) and Collagenase I (Cat. No. 1904MG100, BioFROXX) at 37°C for 30 min. Then, the enzymatic process was terminated by equal volumes of α-MEM medium containing 10% FBS (BI). The suspension was filtered through a 100 μm cell strainer (Life Sciences, USA) and washed twice with the following culture medium: α-MEM medium with 10% FBS, 3 ng/ml Recombinant Murine Epidermal Growth Factor (Cat. no. 315-09, Pepro Tech), 100 mIU/ml Follicle Stimulating Hormone for Injection (Harbin Sanma Animal Pharmaceutical Co. LTD), and 1.5 U/ml chorionic gonadotrophin for injection and 1%

PS. Cells were resuspended in 200 µl culture medium after centrifugation and then mixed well with the bioink for printing.

2.7. Printing of POCs-laden structure and culturing in vitro

A porous circular grid 3D scaffold (nozzle diameter was 340 µm, nozzle temperature was 20°C, and platform temperature was 4°C) was printed using a bioprinting system (Bio-Architect®-WS; Hangzhou Regenovo Biotechnology, Ltd.). During printing, the pneumatic pressure (0.18 – 0.32 kPa) was adjusted to match the best nozzle scanning speed (6 mm). The bioink mixed with the POCs (1×10^6 cells/ml) was used to print. After printing, the POCs-laden 3D scaffolds (2 mm in height and 5 mm in diameter) were soaked in 5% calcium chloride solution (3 min) for cross-linking. Then, the POCs-laden 3D scaffolds were cultured in an incubator (37°C, 5% CO_2), and the POCs viability in the 3D scaffolds was tested with a live/dead assay kit (Molecular Probes, Inc., Cat. No. L3224) on the 1st, 7th, and 14th day. Then, the cells were reviewed under a laser confocal microscope (Zeiss, Germany).

2.8. In vivo study: Female castrated mice model and grouping

The castrated mice model was performed as previously described[9]. Briefly, the mice with a regular oestrum cycle phase were operated on both sides of the back 1.0 cm incisions after being anesthetized successfully. The incisions were made over the ovaries location through the subcutaneous layers. Then, ovaries were removed from the top of the uterine horns and sutured the skin at the incision site. Two weeks after the operation, the vaginal orifice of ovariectomized mice was examined to determine whether the operation was successful or not. The incisions on both sides of the back of the mice were reopened and bluntly stripped to form a tunnel under the skin. The prepared grafts were implanted, and the incisions were sutured with absorbable sutures (Shanghai Pudong Jinhuan Medical Products Co., LTD).

Twenty mice were randomly divided into five groups (four mice in each group): (i) Sham-operated mice as the non-ovariectomized (OVX) group; (ii) ovariectomized mice without further treatment as the OVX-C group; (iii) ovariectomized mice receiving 3D scaffolds ($8 \times 8 \times 3$ mm^3) without cells as the 3D scaffold group; (iv) ovariectomized mice receiving 3D scaffolds with POCs (1×10^7 cells/ml) as the 3D scaffold encapsulating POCs group; and (v) ovariectomized mice receiving the bioink with POCs without printing as the hydrogel encapsulating POCs group.

2.9. Functional evaluation

(1) Neoangiogenesis and cell proliferation

Three weeks after the surgery, vaginal smear was carried out with normal saline that was used to observe the change of each stage of the estrous cycle of the experimental mice. After 4 weeks of treating, the transplants were removed and routinely embedded them in paraffin and sectioned continuously. To evaluate the vascularization and cell proliferation of grafts in the above groups, IHC staining of a rabbit polyclonal antibody against the neovascular-specific cell surface markers CD31 (1:200; Servicebio Technology Co., Ltd., Cat. No. GB11063-2) and a rabbit polyclonal antibody Ki67 (1:100; Wanleibio Co.,Ltd., Cat. No. WL0280a) was performed. In addition, representative sections were stained with TUNEL following the manufacturer protocol (Servicebio™ Fluorescein Tunel Cell Apoptosis Detection Kit) to assess the survival of POCs in vivo.

(2) Sex hormones secretion

Blood samples were collected by eyeball on day 28 after transplantation. Then, the serum was separated overnight at 4°C. All blood samples were, then, immediately stored at −80°C until further analysis. The serum levels of estradiol (E_2), follicle stimulating hormone (FSH), and progesterone (P) were measured using a competitive enzyme-linked immunosorbent assay kit (CUSABIO). The sensitivity for E_2, FSH, and P kits was 40 pg/ml, 2.5 mIU/ml, or 2.5 mIU/ml, respectively.

(3) Expression of POCs markers

To assess the specific markers of the POCs on the implanted grafts, immunofluorescence staining was done. The sections obtained from the above were dewaxed to water and rinsed in PBS (5 min). To reduce the non-specific background, the sections were soaked in 0.3% bovine serum albumin solution for 30 min. Then, the sections were stained using estrogen receptor alpha (ER-α, 1:200; Biosynthesis Biotechnology Co., Ltd., Cat. No. bs-0725R), progesterone receptor (PR, 1:200; Biosynthesis Biotechnology Co., Ltd., Cat. No. bs-23376R), inhibin alpha (Inhibin-α, 1:200; Biosynthesis Biotechnology Co., Ltd., Cat. No. bs-1032R), and anti-FSH-R pAb (FSHR, 1:200; Servicebio Technology Co., Ltd., Cat. No. GB11275-1). The secondary antibody used was Alexa Fluor® 488 Goat Anti-Rabbit antibody (1:200; Invitrogen, CA), and counterstained with DAPI.

2.10. Statistical analysis

SPSS version 21.0 was used. Continuous variables are represented by mean ± standard deviation. The DNA content and IOD value were analyzed by a Student's

t-test. For analyzing the hormone levels and the IOD value of CD31 of various groups, one-way analysis of variance following the LSD method between groups was performed. $P < 0.05$ was considered as a significant difference.

3. Results

3.1. Biochemical characterization of dECM

Decellularization of the ovary ECM is to minimize the loss and damage of ECM, while maximizing the removal of cellular materials. After physical and chemical treatment, the ovary color changed from red to white (**Figure 1A**). We analyzed the DNA content in native and decellularized tissues to assess the decellularization efficiency. As shown in **Figure 1B**, no DNA strip appeared in the dECMs, and DNA quantification showed that the DNA strips in the dECMs were significantly reduced (861.838 ± 18.06 vs. 48.48 ± 1.88 ng/mg, $P < 0.0001$). At the same time, H&E staining and DAPI staining confirmed that no cellular material remained after decellularization (**Figure 1C**). Next, Masson staining and TB staining were performed to assess collagen and proteoglycan in the dECMs. As shown in **Figure 1D**, the compositions of the dECMs and native tissues share a very basic similarity. SDS-PAGE showed that there were various proteins in the dECMs (**Figure 1E**). SEM revealed that the dECMs had no residual cellular components and the fiber orientation and structure were hardly affected (**Figure 1F**).

3.2. Characterization and biocompatibility of the bioink

The generation of 3D ovarian tissue construction includes ovarian tissue decellularization, bioink preparation, and 3D bioprinting (**Figure 2**). Among them, the bioink is particularly important. SEM showed the bioink with a porous reticular microarchitecture (**Figure 3A**). Porous diameters were measured to be 75.58 ± 35.64 μm. The results of CD spectrum (**Figure 3B**) indicated that the bioink had a typical collagen triple helical conformation, showing an inverted S-shaped curve (the maximum positive and negative absorption peaks at 225 nm and 199 nm, respectively). From the thermal denaturation curve, it was known that the unwinding of the triple helix structure mainly occurred between 45°C and 70°C, and Tm was 59°C.

The rheological properties of the dECM solution and the bioink are shown in **Figure 3C**. Both the G' value of the dECM solution and the bioink were significantly higher than G", showing solid-like properties. G' value of the

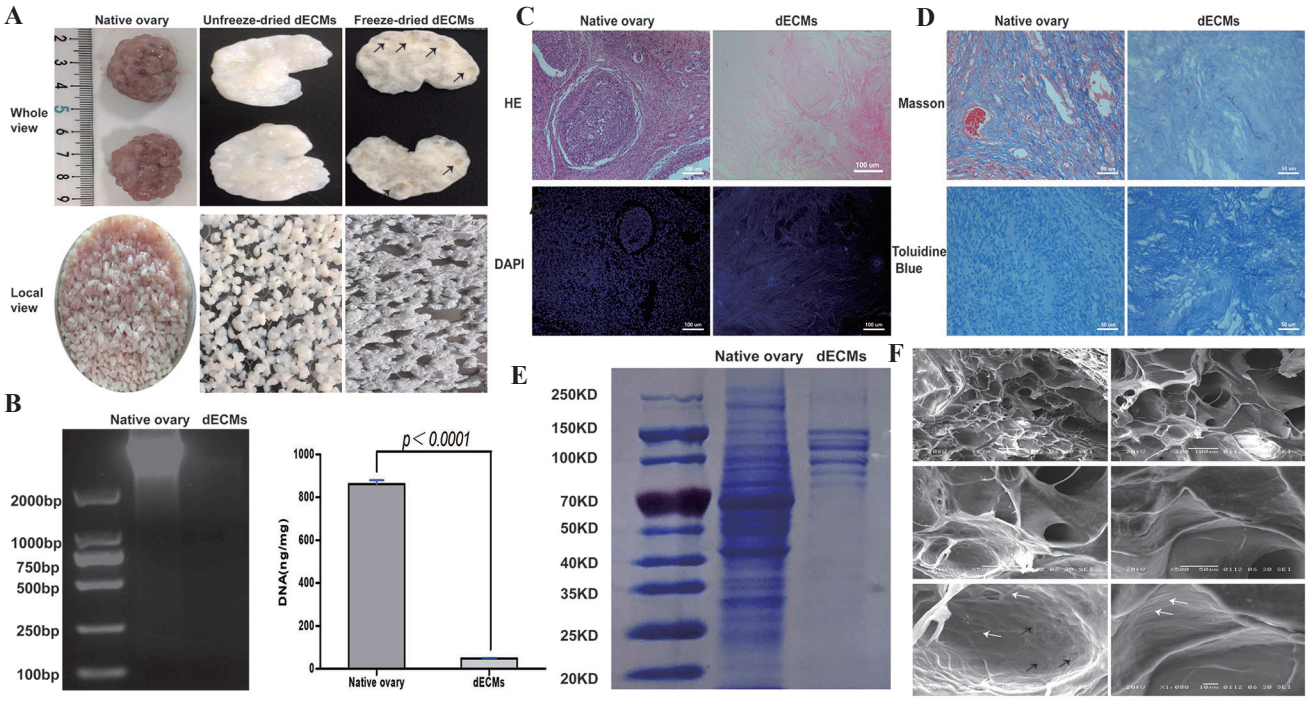

Figure 1. Biochemical characterization of decellularized extracellular matrices (dECMs). (A) Freeze-dried ECM was tough and follicular cavities were observed (black arrows). (B) DNA content analysis. (C) H&E staining and DAPI staining showed that there were no residual cellular materials after decellularization. (D) Masson staining and TB staining showed that there were collagen and proteoglycan in the dECMs. (E) SDS-PAGE revealed the existence of various proteins within the dECMs. (F) Microarchitecture of decellularized ovary matrix by SEM. The extracellular matrix structure was intact. Collagen (white arrow) and flexible fibronectin fibers (black arrow) were found in the pore wall.

Figure 2. The preparation of ovary-derived decellularized extracellular matrix (dECM)-based bioink and the printing of porous cylindrical 3D scaffold constructs.

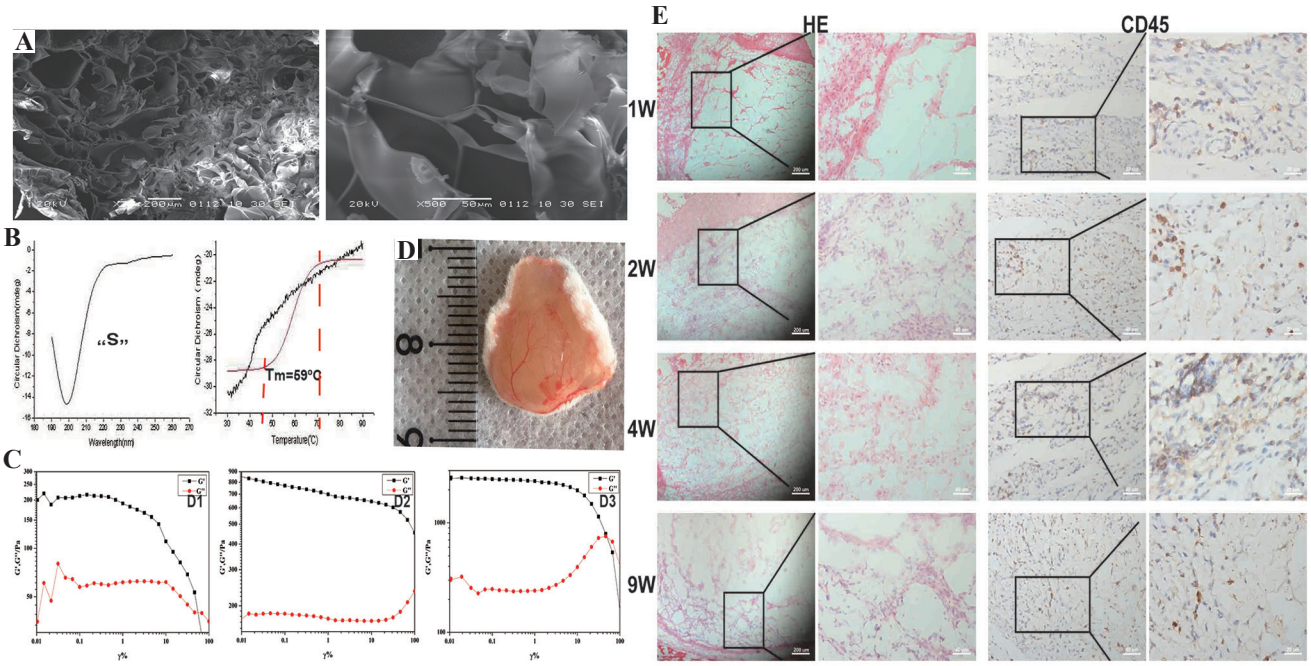

Figure 3. Characterization and biocompatibility of the dECMs-based bioink. (A) Microarchitecture of the bioink by SEM. (B) Circular dichroism spectrum was used to determine the protein structure and thermal stability of the bioink. (C) Rheological properties were measured to assess the mechanical properties of the bioink before (D2) and after (D3) cross-linking of calcium chloride compared with those of dECM solution (D1). (D) Blood vessels were clearly visible on 1 week after implantation. (E) The biocompatibility of the bioink was assessed by H&E staining and CD45 (a marker for inflammatory cells) immunostaining.

cross-linked bioink (D3, about 2414 Pa) was significantly higher than those of the uncross-linked bioink (D2, about 739 Pa) and dECM solution (D1, about 190 Pa).

Biocompatibility of bioinks in vivo was evaluated by subcutaneous xenotransplantation. All mice were free of any complications within 9 weeks of implantation. At 1st week, a potent angiogenesis response could be seen on the bioink tissues surface (**Figure 3D**). H&E staining showed that there were numerous inflammatory cells 1 week after implantation, principally aggregated in the

junction of the skin and the bioink. During the 2nd week, inflammatory cells increased in the bioink. However, from the 2nd to 9th week, the total amount of inflammatory cells decreased, and the volume of bioink injected in the 9th week was significantly lower than that in the 1st week. Furthermore, the expression of CD45 (identify the inflammatory cells) was similar to the H&E staining results (**Figure 3E**).

3.3. Viability of POCs in the 3D scaffold in vitro

As shown in **Figure 4A**, the isolated POCs included a large number of stromal cells and follicles at different developmental stages. After culturing 2 weeks, the 3D scaffolds maintained their original shape, but appeared softer than they were in the beginning. On the other hand, the shear force generated during printing and residual chemicals in the dECM-based bioink may affect cellular viability. Therefore, the live/dead assay was performed to assess the survival status of the laden POCs. The assay showed that the POCs in the 3D scaffolds showed high cell viability on the 1st day (>95%) and remained around 90% on the 14th day (**Figure 4B**).

3.4. In vivo evaluation of the printed ovarian tissue constructs

Four weeks after implantation, macroscopic observations showed a slower degradation of scaffolds compared with hydrogel, the above constructs maintained their shape, and functional blood vessels were developed (**Figure 5**). IHC results demonstrated the transplanted tissues had neovascularization (**Figure 6A-C**, red arrows). The positive signal of CD31 increased significantly in the group of 3D scaffold encapsulating POCs (0.0063 ± 0.0011) than in the other groups (0.0016±0.0009 in the hydrogel encapsulating POCs group and 0.0032 ± 0.0008 in the 3D scaffold group (P = 0.000 and 0.001). The expression of CD31 in the hydrogel encapsulating POCs group was lower than the 3D scaffold group (P = 0.042) (**Figure 6G**).

POCs were immune stained with Ki67 to evaluate the cell proliferation (**Figure 6D-F**). More positive Ki67 signals (cells in brown) were detected in the 3D scaffold encapsulating POCs group (0.0074 ± 0.0017) than in the hydrogel encapsulating POCs group (0.0036 ± 0.0010 (P = 0.001) (**Figure 6G**). TUNEL staining was used to evaluate the cell apoptosis in the grafted tissues. The numbers of TUNEL-positive cells in both groups were similar (**Figure 6H**).

Hormone evaluation showed that the levels of serum E_2 increased significantly in the 3D scaffold encapsulating POCs group (465.91 ± 24.77 pg/ml) than those in the OVX-C group (332.28 ± 26.17 pg/ml, P = 0.000) and in the 3D scaffold group (390.06 ± 41.47 pg/ml, P = 0.014) and were close to those in the non-OVX group (494.31 ± 35.96 pg/ml, P = 0.292) and in the hydrogel encapsulating POCs group (424.69 ± 24.26 pg/ml, P =0.138). In the 3D scaffold encapsulating POCs group, implantation led to the restoration of FSH (44.69 ± 24.17 mIU/ml) and P (2.55 ± 1.34 ng/ml) to the physiological level (FSH: 50.34 ± 2.73 mIU/ml; P: 3.35 ± 2.56 ng/ml). Serum P levels in the 3D scaffold group (12.75 ± 2.59 ng/ml) and the hydrogel encapsulating POCs group (14.52 ± 3.02 ng/ml) were similar to those of the OVX-C mice (12.75 ± 2.59 ng/ml). Serum E_2 and FSH levels in the group of 3D scaffold and hydrogel encapsulating POCs did not restore up to the physiological level compared to non-OVX group, although their serum E_2 and FSH levels were improved (**Figure 7A-C**).

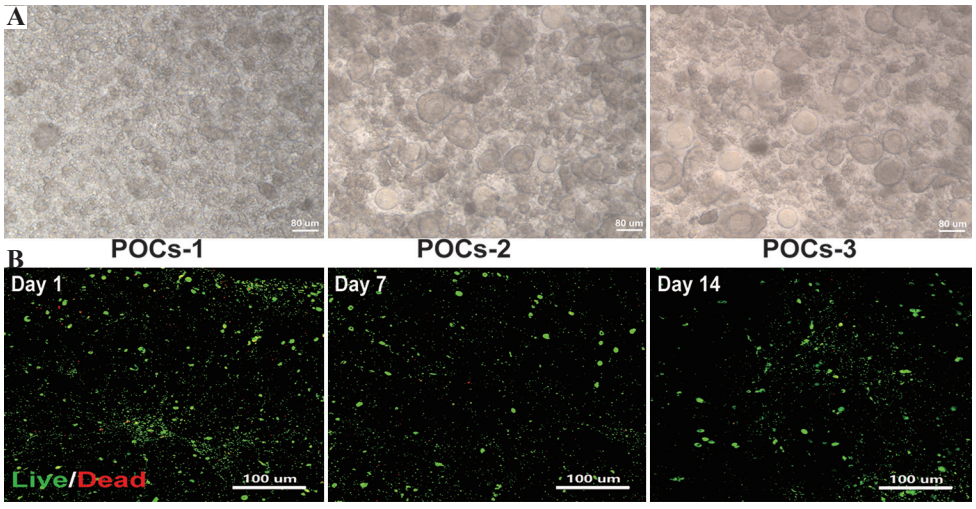

Figure 4. Viability of primary ovarian cells (POCs) in the 3D scaffold in vitro. (A) The isolated POCs included a vast majority of stromal cells (POCs-1) and a large number of follicles at different developmental stages (POCs-2 and POCs-3). (B) Using the live/dead assay to examine the POCs survival in the 3D scaffolds in vitro. Green fluorescence refers to living cells containing calcein AM, while red fluorescence refers to dead cells containing EthD-1.

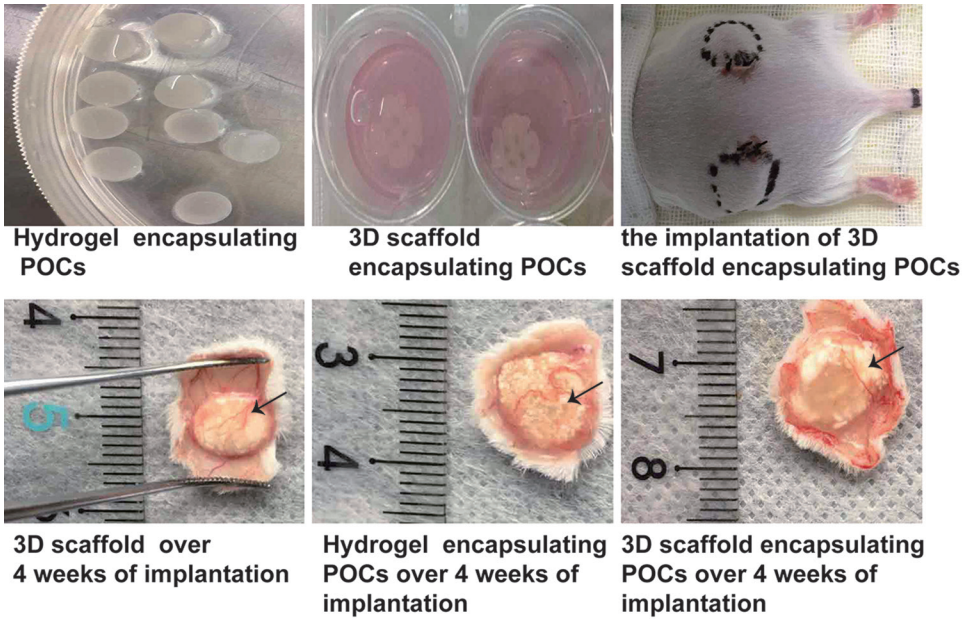

Figure 5. General view of grafts before and after transplantation. At 4 weeks after implantation, the constructs maintained their shape and developed functional blood vessels (black arrow).

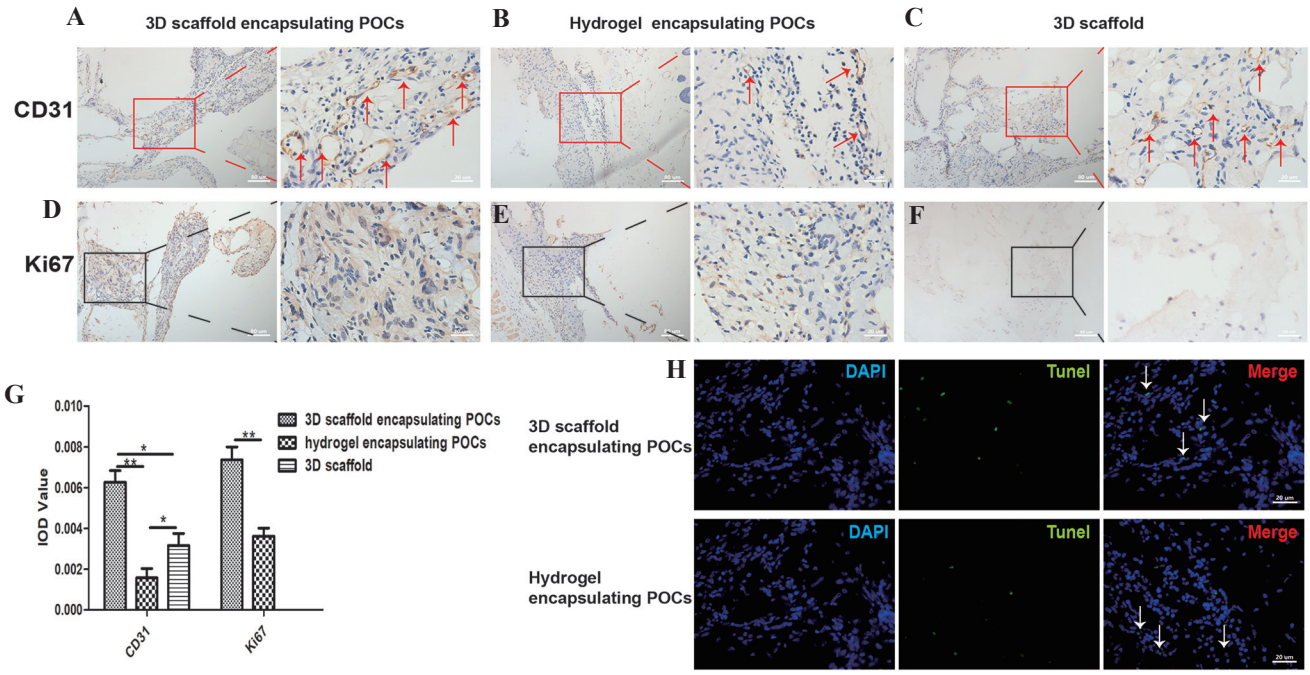

Figure 6. Evaluation of the neoangiogenesis and cell proliferation. (A-C) The effects of 3D scaffolds, 3D scaffold encapsulating POCs, and hydrogel encapsulating POCs constructs on blood revascularization (CD31, red arrows). (D-F) Immunostaining for the cell proliferation-specific marker (Ki67, cells in brown), in the implanted 3D scaffold encapsulating POCs and hydrogel encapsulating POCs constructs. (G) Expression of CD31, Ki67. *$P < 0.05$, **$P < 0.0001$. (H) Identification of the apoptosis of sections from grafts treated with 3D scaffold encapsulating POCs and hydrogel encapsulating POCs (white arrows).

However, vaginal smear observations did not perfectly coincide with these findings. The estrous cycle of mice in the OVX-C group rested on anestrus for a long time that were called estrous cycle inhibition. The results of the 3D scaffold and the hydrogel encapsulating POCs groups were similar (a large number of leukocyte and a fraction of epithelial cells). High level of anestrus was observed in the 3D scaffold encapsulating POCs group,

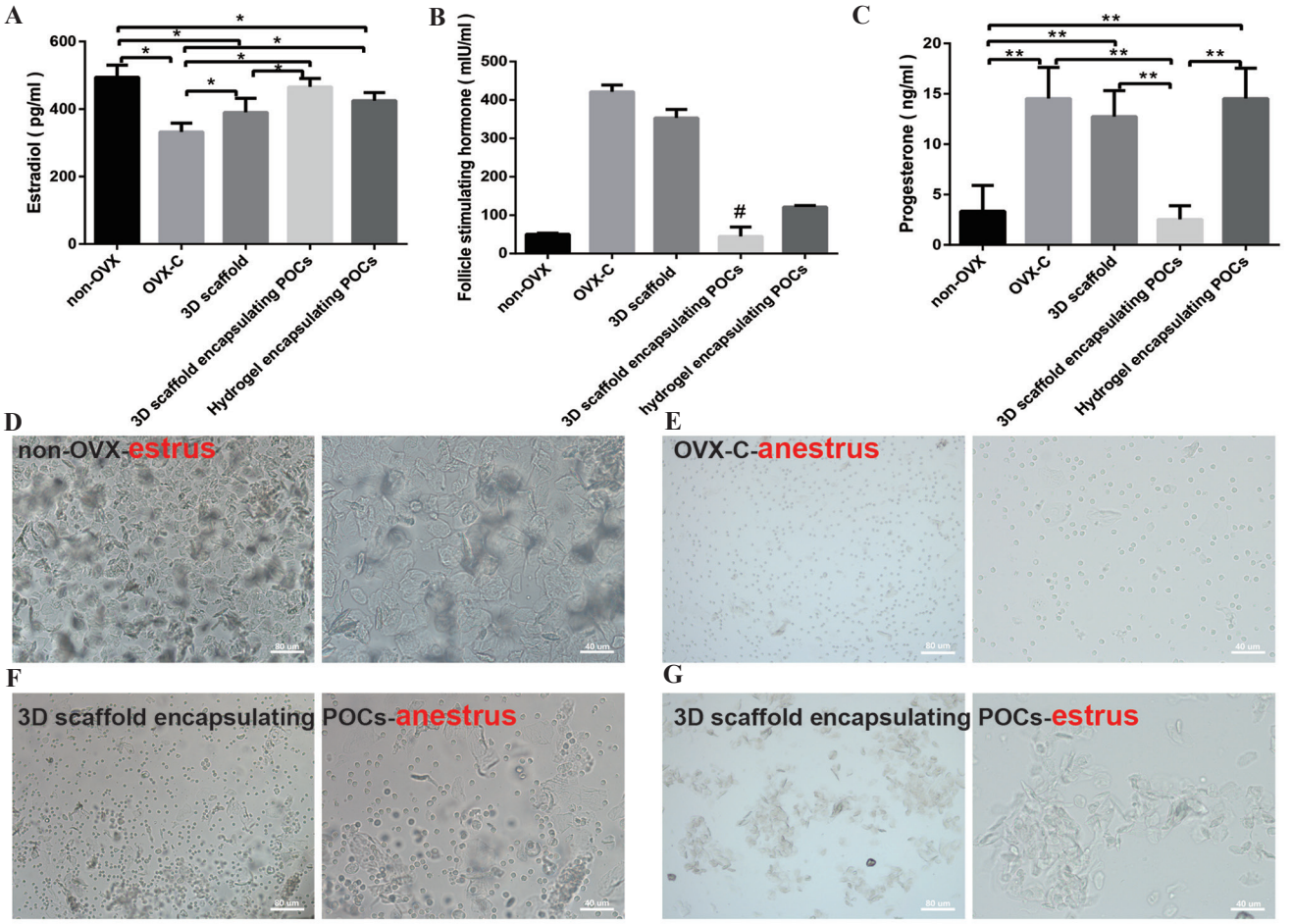

Figure 7. Hormone assessment and the vaginal smear. (A-C) The comparison of serum hormone levels of samples from five different groups. *$P < 0.05$, **$P < 0.0001$. # means statistical differences exist in pairwise comparison between the groups ($P \leq 0.001$), but not in the 3D scaffold encapsulating POCs group vs. non-OVX group ($P = 0.684$). (D-G) The vaginal smear at 4 weeks after implantation. (D) A large number of keratinized cells can be observed in the non-OVX group mice on estrus. (E) The OVX-C group mice were on anestrus for a long time, and a large number of leukocytes can be seen. (F) A high level of anestrus was observed in three mice of the 3D scaffold encapsulating POCs group. (G) A lower level of estrus in one mice of the 3D scaffold encapsulating POCs group was observed.

and the mature vaginal epithelia (less than that of non-OVX mice) reappeared in one mouse of the 3D scaffold encapsulating POCs group (**Figure 7D-G**).

On the other hand, the study assessed the expression of germ cells, including ER-α, PR, inhibin-α and FSHR, in samples from the 3D scaffold encapsulating POCs group and hydrogel encapsulating POCs group (**Figure 8A-D**). The positive cells of the germ cells were observed in the two groups, and they were both significantly higher in the group of 3D scaffold encapsulating POCs than in the group of hydrogel encapsulating POCs (ER-α; 0.0072 ± 0.0020 vs. 0.0049 ± 0.0014, $P = 0.02$; Inhibin-α; 0.0065 ± 0.0025 vs. 0.0041 ± 0.0015, $P = 0.043$; FSHR; 0.007 ± 0.0019 vs. 0.0046 ± 0.0018, $P = 0.037$), but there was no significant difference in the expression of PR (0.0061 ± 0.0020 vs. 0.0038 ± 0.0014, $P = 0.124$) between these groups (**Figure 8E**).

4. Discussion

This study shows that the 3D POCs-laden structures can support the long-term survival of POCs in vitro and in vivo. The female castrated mouse model demonstrated that the 3D scaffolds encapsulating POCs were beneficial to improve ovarian function. Although estrus was observed in only one mouse by vaginal smears, the 3D scaffold encapsulating POCs construct initiated puberty in the ovariectomized mice.

ECM supports tissue formation specific to the implant site for structural remodeling rather than dysfunctional scar tissue formation[18]. Early studies have proven that tissue-specific ECM bioscaffolds can aid in the recovery of injured tissue function[8] and tissue formation[19,20], which underscores the advantages of tissue specificity. It is known that once the cellular material remaining in the ECM is transplanted into the recipient, an immune

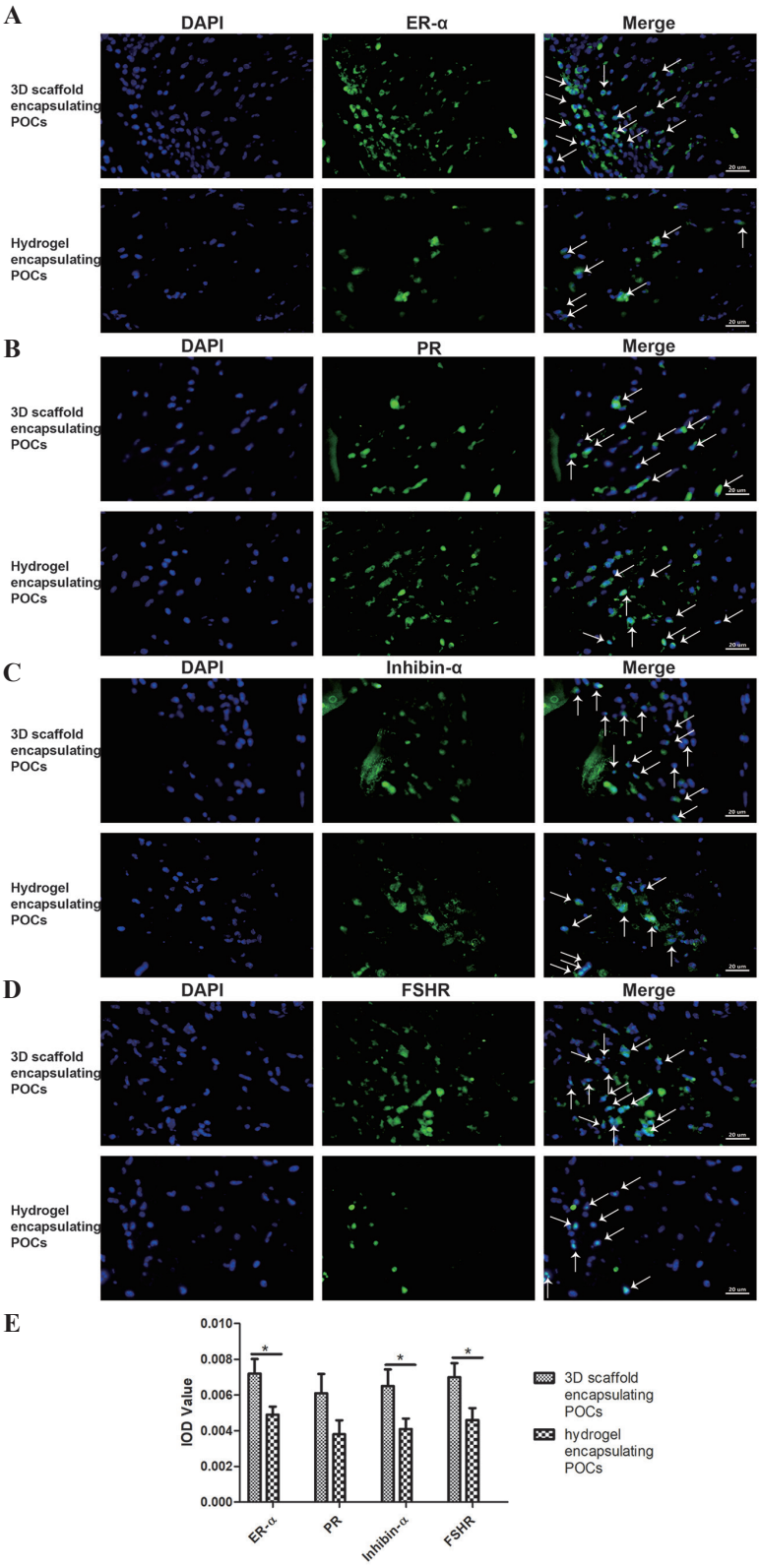

Figure 8. Detection of the expression of ER-α, PR, inhibin-α and FSHR within the 3D scaffold encapsulating POCs and hydrogel encapsulating POCs constructs after 4-week implantation. DAPI located in the nucleus (blue), the specific primary antibody located in the cell membrane and cytoplasm (green). Green and blue superimposed to appear white, representing the expression of steroid hormone receptors in the groups (white arrows). The expression of ER-α, Inhibin-α and FSHR were more in the 3D scaffold encapsulating POCs group than in the hydrogel encapsulating POCs group. However, there was no significant difference in the expression of PR ($P = 0.12$). *$P < 0.05$.

response will be triggered[21]. It has been shown that if the DNA content in the ECM is less than 50 ng/mg[22] it does not trigger an immune response, but promotes tissue remodeling[23]. Our results meet this criterion and indicate the suitability for implantation. Another challenge in decellularization is to retain as much of the ECM components as possible while effectively removing the cells. Collagen fibers and proteoglycans are the major components of the basement membrane[24], and their presence, further, demonstrates that the decellularization process preserves the major components of the ECM. An intact basement membrane is important for tissue growth and differentiation[25]. Several studies have identified more than 200 unique protein molecules present in the decellularized human vocal fold scaffolds[26]. Our study also confirmed the presence of proteins in the decellularized ovarian tissue, which would guarantee the advantages of bioink 3D scaffolds based on dECMs. Indeed, decellularized ovarian tissue has been shown to preserve 3D follicular structures and support follicle development in vivo[9-12].

However, the dECMs often lack tailored microgeometry[27], resulting in cell distribution confined to the surface of the material, with only a fraction of cells infiltrating the internal regions[28]. Furthermore, once implant the dECMs, the cells infiltrated, or seeded on the dECMs are mainly sustained by the diffusion of oxygen and nutrients before forming a vascular network[29]. The above problems can be resolved by 3D bioprinting technology. The 3D-bioprinted cell-loaded scaffolds have an ideal spatial distribution. Thus, the deposition of bioink can be precisely controlled (down to the micron) to form tissue ultrastructure[30]. The 3D scaffold retains its 3D ultrastructure before degradation. Besides provides the location of the substrate, it also determines the spatial distribution of the loaded cells[31], and then creates a suitable living environment for the cells. After the 3D-printed scaffold loses its physical support, the cells in the scaffold can build their own ECM locally by secreting matrix proteins, enabling finer tissue remodeling. Furthermore, several studies have shown that 3D scaffolds with 50–200 μm pores could not only promote cell proliferation, migration, and infiltration, but also promote tissue regeneration and repair through loading more cells[16,32]. The higher survival rate of POCs within the 3D scaffolds during first 2 weeks of in vitro culture suggests that the use of porous 3D scaffolds with dECM-based bioink allows sufficient nutrient and oxygen delivery to the cells within the grafts, making long-term in vitro culture become possible.

As we all known, dECM has poor mechanical properties. The previous studies have used polycaprolactone (PCL) to assist adipose tissue in dECM to print 3D scaffolds[33]. However, if the mechanical properties of 3D-bioprinted structures do not match with the natural tissue (PCL is stiffer than adipose tissue), this can lead to complication. Therefore, using a lower stiffness material or an appropriate strategy to match, the mechanical properties seem to be more suitable than using PCL in the 3D-bioprinted structural design. Therefore, we mixed the dECM solution with the seaweed gelatin blend solution to match the mechanical properties of natural tissues. The hardness of the bioink is increased by chemical cross-linking of the seaweed with divalent cations such as Ca^{2+} or Sr^{2+}. Gelatin has high viscosity and easy freezing properties, and it is homologous to collagen[34]. The dECM-based bioink conformed to the typical collagen triple helix conformation and remained stable at physiological temperature. After printing, the mechanical properties of the 3D scaffolds were enhanced by calcium ion cross-linking and maintained an open porous 3D structure, allowing nutrients transfer for tissue remodeling.

The biocompatibility of the dECM-based bioink must first be evaluated before assessing the role of 3D bioprinting structures in vivo, which is one of the great concerns in regenerative medicine[35]. We observed that the inflammation elicited by the injected bioink gradually decreased with the passage of time. It shows the bioink with an ability that performs an appropriate host response in the specific application. Meanwhile, the live/dead assay also shows that the bioink is non-cytotoxic. From these, we can conclude that the dECM-based bioink has good biocompatibility.

In vivo testing of 3D scaffolds, 3D scaffolds encapsulating POCs, and hydrogels encapsulating POCs in the female castrated mouse model yielded some interesting results. Bioink in a normal subcutaneous mice induced a strong angiogenic response at 1 week after implantation and promoted the migration of inflammatory cells at 2 weeks, possibly due to proteolytic stimulation of cell migration by the bioink or increased availability of major angiogenic growth factors during bioink degradation[36]. Neovascularization of implanted structures is an important indicator for in vivo studies. There is considerable synergistic effect of POCs and decellularized ovarian tissue on angiogenesis of implanted structures. As reported elsewhere, stromal cells in POCs can promote angiogenesis[3,10,37]. However, neovascularization was also observed in the 3D scaffold group. It has been reported that dECM has the potential capacity for angiogenesis[38]. Thus, decellularized ovarian tissues may induce angiogenesis from the peri-host tissue to the grafts. Macroscopically, in the 4-week study, the volume of the hydrogels encapsulating POCs decreased more rapidly than those of the 3D scaffolds and the 3D scaffolds encapsulating POCs in the 4-week study. This suggests that the 3D-printed scaffolds have a relatively

slow degradation rate, thus maintaining the volume of the graft structure and allowing tissue regeneration.

Notably, the artificial ovaries are designed to mimic the two representative functions of the native ovaries: Egg production and sex hormones secretion[39]. Therefore, we assessed the survival and proliferation of POCs within the bioink at 4 weeks after implantation. Only a few cells were TUNEL positive, indicating a high survival rate of POCs in the artificial ovaries. A high rate of Ki67-positive cells was also found, indicating that 3D POCs-laden structures can support the proliferation of POCs. Meanwhile, serum levels of sex hormones were significantly increased and germ cell receptors were expressed, with estrus observed by vaginal smear in one ovariectomized mouse treated with 3D POCs-laden scaffold. Moreover, the printed constructs were more strongly expressed (neovascularization, cell proliferation, and germ cell receptors) than the non-printed constructs, confirming the advantages of 3D bioprinting.

5. Conclusion

This work shows that dECM-based bioink offers a new approach to fabricate bionic 3D structures. 3D POCs-laden structures play an important role in repairing damaged ovarian function, and it is a promising method for fertility preservation. Conceivably, with the development of 3D bioprinting technology and the complementarity between multiple disciplines, 3D-bioprinted cell structures may become an effective treatment for patients with ovarian insufficiency.

Acknowledgment

The authors would like to thank all members of the Department of Central Laboratory at the Second Hospital of Hebei Medical University for their scientific advice and encouragement and Dr. Wang Binglei at the Department of Neurology for his help in drafting the manuscript.

Funding

This work was financially supported by the National Natural Science Foundation of China (No. 8167060210) and the Natural Science Foundation of Hebei Province (No. H2021206463).

Conflict of interest

The authors declare that they have no conflicts of interests.

Author contributions

J.Z. and X.H. designed research, performed and analyzed experiments, prepared figures, and drafted the manuscript. Y.L., C.H., Z.L., S.Y., X.L., L.Z. and J.G. provided key reagents and insightful discussion. X.H. and J.Z. supervised the study and wrote the manuscript. All authors edited the manuscript.

References

1. Siegel RL, Miller KD, Fuchs HE, 2021, Cancer Statistics, 2021. *CA Cancer J Clin*, 71:7–33. https://doi.org/10.3322/caac.21654
2. Dolmans MM, Luyckx V, Donnez J, *et al.*, 2013, Affiliations Expand Risk of Transferring Malignant Cells with Transplanted Frozen-thawed Ovarian Tissue. *Fertil Steril*, 99:1514–22. https://doi.org/10.1016/j.fertnstert.2013.03.027
3. Dath C, Dethy A, Van Langendonckt A, *et al.*, 2011, Endothelial Cells are Essential for Ovarian Stromal Tissue Restructuring after Xenotransplantation of Isolated Ovarian Stromal Cells. *Hum Reprod*, 26:1431–9. https://doi.org/10.1093/humrep/der073
4. Rodgers RJ, Irving-Rodgers HF, Russell DL, 2003, Extracellular Matrix of the Developing Ovarian Follicle. *Reproduction*, 126:415–24. https://doi.org/10.1530/rep.0.1260415
5. Chiti MC, Dolmans MM, Mortiaux L, *et al.*, 2018, A Novel Fibrin-based Artificial Ovary Prototype Resembling Human Ovarian Tissue in Terms of Architecture and Rigidity. *J Assist Reprod Genet*, 35:41–8. https://doi.org/10.1007/s10815-017-1091-3
6. Day JR, David A, Cichon AL, *et al.*, 2018, Immunoisolating Poly(Ethylene Glycol) based Capsules Support Ovarian Tissue Survival to Restore Endocrine Function. *J Biomed Mater Res A*, 106:1381–9. https://doi.org/10.1002/jbm.a.36338
7. Amorim CA, Shikanov A, 2016, The Artificial Ovary: Current Status and Future Perspectives. *Future Oncol*, 12:2323–32. https://doi.org/10.2217/fon-2016-0202
8. Sellaro TL, Ranade A, Faulk DM, *et al.*, 2010, Maintenance of Human Hepatocyte Function in vitro by Liver-derived Extracellular Matrix Gels. *Tissue Eng Part A*, 16:1075–82. https://doi.org/10.1089/ten.TEA.2008.0587
9. Laronda MM, Jakus AE, Whelan KA, *et al.*, 2015, Initiation of Puberty in Mice Following Decellularized Ovary Transplant. *Biomaterials*, 50:20–9. https://doi.org/10.1016/j.biomaterials.2015.01.051
10. Liu WY, Lin SG, Zhuo RY, *et al.*, 2017, Xenogeneic Decellularized Scaffold: A Novel Platform for Ovary Regeneration. *Tissue Eng Part C Methods*, 23:61–71. https://doi.org/10.1089/ten.TEC.2016.0410
11. Hassanpour A, Talaei-Khozani T, Kargar-Abarghouei E, *et*

al., 2018, Decellularized Human Ovarian Scaffold based on a Sodium Lauryl Ester Sulfate (SLES)-treated Protocol, as a Natural Three-dimensional Scaffold for Construction of Bioengineered Ovaries. *Stem Cell Res Ther*, 9:252. https://doi.org/10.1186/s13287-018-0971-5

12. Pors SE, Ramløse M, Nikiforov D, *et al*., 2019, Initial Steps in Reconstruction of the Human Ovary: Survival of Pre-antral Stage Follicles in a Decellularized Human Ovarian Scaffold. *Hum Reprod*, 34:1523–35. https://doi.org/10.1093/humrep/dez077
13. Chiti C, Viswanath A, Vanacker J, et al., 2016, Development of a Transplantable Artificial Ovary: Influence of Follicle Stage on Transplantation Outcome. In: Front Bioeng Biotechnol, Conference Abstract: 10th World Biomaterials Congress. https://doi.org/10.3389/conf.FBIOE.2016.01.00699
14. Moroni L, Boland T, Burdick JA, *et al*., 2018, Biofabrication: A Guide to Technology and Terminology. *Trends Biotechnol*, 36:384–402. https://doi.org/10.1016/j.tibtech.2017.10.015
15. Groll J, Burdick JA, Cho DW, *et al*., 2018, A Definition of Bioinks and their Distinction from Biomaterial Inks. *Biofabrication*, 11:013001. https://doi.org/10.1088/1758-5090/aaec52
16. Abaci A, Guvendiren M, 2020, Designing Decellularized Extracellular Matrix-Based Bioinks for 3D Bioprinting. *Adv Healthc Mater*, 9:e2000734. https://doi.org/10.1002/adhm.202000734
17. Hou CX, Zheng JH, Li ZK, *et al.*, 2021, Printing 3D Vagina Tissue Analogues with Vagina Decellularized Extracellular Matrix Bioink. *Int J Biol Macromol*., 180:177–86. https://doi.org/10.1016/j.ijbiomac.2021.03.070
18. Badylak SF, 2004, Xenogeneic Extracellular Matrix as a Scaffold for Tissue Reconstruction. *Transpl Immunol*, 12:367–77. https://doi.org/10.1016/j.trim.2003.12.016
19. Petersen TH, Calle EA, Zhao L, *et al*., 2010, Tissue-engineered Lungs for in vivo Implantation. *Science*, 329:538–41. https://doi.org/10.1126/science.1189345
20. Uygun BE, Soto-Gutierrez A, Yagi H, *et al*., 2010, Organ Reengineering Through Development of a Transplantable Recellularized Liver Graft using Decellularized Liver Matrix. *Nat Med*, 16:814–20. https://doi.org/10.1038/nm.2170
21. Crapo PM, Gilbert TW, Badylak SF, 2011, An Overview of Tissue and whole Organ Decellularization Processes. *Biomaterials*, 32:3233–43. https://doi.org/10.1016/j.biomaterials.2011.01.057
22. Caralt M, Uzarski JS, Iacob S, *et al*, 2015, Optimization and Critical Evaluation of Decellularization Strategies to Develop Renal Extracellular Matrix Scaffolds as Biological Templates for Organ Engineering and Transplantation. *Am J Transplant*, 15:64–75. https://doi.org/10.1111/ajt.12999
23. Badylak SF, Gilbert TW, 2008, Immune Response to Biologic Scaffold Materials. *Semin Immunol*, 20:109–16. https://doi.org/10.1016/j.smim.2007.11.003
24. Heeren AM, Iperen LV, Klootwijk DB, *et al*., 2015, Fernandes Development of the Follicular Basement Membrane during Human Gametogenesis and Early Folliculogenesis. *BMC Dev Biol*, 15:4. https://doi.org/10.1186/s12861-015-0054-0
25. Streuli C, 1999, Extracellular Matrix Remodelling and Cellular Differentiation. *Curr Opin Cell Biol*, 11:634–40. https://doi.org/10.1016/s0955-0674(99)00026-5
26. Welham NV, Chang Z, Smith LM, *et al*., 2013, Proteomic Analysis of a Decellularized Human Vocal Fold Mucosa Scaffold using 2D Electrophoresis and High-resolution Mass Spectrometry. *Biomaterials*, 34:669–76. https://doi.org/10.1016/j.biomaterials.2012.09.050
27. Turner AEB, Yu C, Bianco J, *et al*., 2012, The Performance of Decellularized Adipose Tissue Microcarriers as an Inductive Substrate for Human Adipose-derived Stem Cells. *Biomaterials*, 33:4490–9. https://doi.org/10.1016/j.biomaterials.2012.03.026
28. Yu C, Bianco J, Brown C, *et al*., 2013, Porous Decellularized Adipose Tissue Foams for Soft Tissue Regeneration. *Biomaterials*, 34:3290–302. https://doi.org/10.1016/j.biomaterials.2013.01.056
29. Wang XH, Yan YN, Zhang RJ, 2007, Rapid Prototyping as a Tool for Manufacturing Bioartificial Livers. *Trends Biotechnol*, 25:505–13. https://doi.org/10.1016/j.tibtech.2007.08.010
30. Vijayavenkataraman S, Yan WC, Lu WF, *et al*., 2018, 3D Bioprinting of Tissues and Organs for Regenerative Medicine. *Adv Drug Deliv Rev*, 132:296–332. https://doi.org/10.1016/j.addr.2018.07.004
31. Ferlin KM, Prendergast ME, Miller ML, *et al*., 2016, Influence of 3D Printed Porous Architecture on Mesenchymal Stem Cell Enrichment and Differentiation. *Acta Biomater*, 32:161–9. https://doi.org/10.1016/j.actbio.2016.01.007
32. Hu K, Cui F, Lv Q, *et al*., 2008, Preparation of Fibroin/Recombinant Human-like Collagen Scaffold to Promote Fibroblasts Compatibility. *J Biomed Mater Res A*, 84:483–90. https://doi.org/10.1002/jbm.a.31440

33. Pati F, Ha DH, Jang J, *et al*., 2015, Biomimetic 3D Tissue Printing for Soft Tissue Regeneration. *Biomaterials*, 62:164–75. https://doi.org/10.1016/j.biomaterials.2015.05.043

34. Lee A, Hudson AR, Shiwarski DJ, *et al*., 2019, 3D Bioprinting of Collagen to Rebuild Components of the Human Heart. Science, 365:482–7. https://doi.org/10.1126/science.aav9051

35. Zor F, Selek FN, Orlando G, *et al*., 2019, Biocompatibility in Regenerative Nanomedicine. *Nanomedicine (Lond)*, 14:2763–75. https://doi.org/10.2217/nnm-2019-0140

36. Brown BN, Freund JM, Han L, *et al*., 2011, Comparison of Three Methods for the Derivation of a Biologic Scaffold Composed of Adipose Tissue Extracellular Matrix. *Tissue Eng Part C Methods*, 17:411–21. https://doi.org/10.1089/ten.TEC.2010.0342

37. Dolmans MM, Amorim CA, 2019, Fertility Preservation: Construction and use of Artificial Ovaries. *Reproduction*, 158:F15–25. https://doi.org/10.1530/REP-18-0536

38. Maghsoudlou P, Georgiades F, Tyraskis A, *et al*., 2013, Preservation of Micro-architecture and Angiogenic Potential in a Pulmonary Acellular Matrix Obtained using Intermittent Intra-tracheal Flow of Detergent Enzymatic Treatment. *Biomaterials*, 34:6638–48. https://doi.org/10.1016/j.biomaterials.2013.05.015

39. Kim YJ, Kim YY, Song DY, *et al*., 2018. Proliferation Profile of Uterine Endometrial Stromal Cells during in vitro Culture with Gonadotropins: Recombinant Versus Urinary Follicle Stimulating Hormone. *Tissue Eng Regen Med*, 16:131–9. https://doi.org/10.1007/s13770-018-0156-4

Publisher's note